SUPPLEMENTARY MATERIALS AND METHODS

Plasmonic Nanobubbles Rapidly Detect and Destroy Drug-Resistant Tumors

Ekaterina Y. Lukianova-Hleb, Xiaoyang Ren, Debra Townley, Xiangwei Wu,

Michael E. Kupferman, Dmitri O. Lapotko

1. Gold nanoparticles. Solid gold spheres with diameters of 20 and 60 nm were obtained from BioAssay Works LLC (Ijamsville, MD). These NPs were covalently conjugated with C225 antibody (Erbitux, ImClone Systems Inc., Branchburg, NJ), an antibody against the epidermal growth factor receptor (EGFR) that is over-expressed by HN31 cancer cells, by BioAssayWorks LLC (Ijamsville, MD). Optical absorption spectra of gold NPs were obtained for suspensions of NPs and their clusters as spectra of optical density. Optical density includes both absorption and scattering components. However, for NPs with a diameter of less than 100 nm, the scattering component is negligibly small and thus optical density was used as a measure of optical absorbance. Ocean Optics Inc spectrometer (USB 650 Red Tide spectrometer, Dunedin, FL) and software were used to compare optical absorbance at different wavelength.

2. PNB generation. We used the duration of the excitation pulse long enough to allow thermally-induced processes in an NP to develop (> 10 ps) and short enough to prevent significant development of the secondary environmental phenomena due to heat transfer (heat dissipation (100-1000 ps), evaporation and bubble expansion (>100 ps) and total destruction of the NP). Use of a single pulse avoided the influence of any irreversible changes in the NP during its interaction with excitation radiation. Therefore, we employed 70 ps pulses with high pulse-to-

pulse energy stability and Gaussian intensity profile at wavelengths close to the recently discovered NIR peak of plasmon resonance of gold spheres (780 nm) that was provided by tunable pulsed laser (PL-2250, Ekspla, Vilnius, Lithuania). The laser beam was directed into a sample through a focusing lens with the beam diameter at the sample plane being 16 μm for cell culture studies and 250 μm for *in vivo* studies. The fluence of each single laser pulse was controlled with a polarizing attenuator and measured by registering the size of the image of the laser beam at the sample plane with an EM CCD camera (Luka model, Andor Technology, Northern Ireland), and the pulse energy was assessed with an energy meter (Ophir Optronics, Ltd., Israel). The diameter of the Gaussian laser beam was measured at the level $1/e^2$ relative to its maximal image pixel amplitude in the center of the beam.

For studying the tumor slices and animals the above set up was modified with two additional options, optical fiber probe and lateral scanning system. Optical fiber probe employed 200 μm multi-mode fiber probe (Polymicro Technologie, Phoenix, AZ) for the delivery of the excitation laser pulse to the surface of the tumor (Figure 4A). Slices and animals were scanned across the fiber tip or across the free-space laser beam by using a motorized microscope stage (8MT167-100, Standa Ltd., Vilnius, Lithuania) that was operated via custom-made LabView modules (National Instruments Corporation, Austin, TX). The scan speed was synchronized to the beam diameter and the pulse repetition rate in order to provide a single laser pulse exposure of the every area of the sample.

3. PNB detection and metrics. PNBs were detected, imaged and measured through three independent methods that were employed simultaneously. Optical detection is based on the excellent light scattering properties of the nanobubbles [S1-S3]. Acoustic detection is based on the generation of the pressure transients during the bubble expansion and collapse, complements

light scattering detection, and, most importantly for diagnostic application, can be used for *in vivo* detection of nanobubbles in opaque tissue.

Optical scattering was employed in the two methods of time-response and time-resolved imaging. Optical scattering time-response (Figure S1B, S2C) was detected with a continuous stabilized 633 nm laser (<0.1 mW, 05-STP-901, CVI Meller Griot, Albuquerque, NM) that was focused onto a sample collinearly to the excitation laser beam. The axial intensity of the probe beam was monitored in a far field after the sample with photodetector (FPD510-FV, Thorlabs Inc., Newton, NJ), whose output was analyzed by digital oscilloscope (Lecroy X42 WaveSurfer, LeCroy Corporation) as the time-response. The duration (not amplitude) of the response is nearly proportional to the maximal diameter of a PNB [S3-S6] and was measured as the PNB lifetime. The maximal diameter, in turn, determines the therapeutic effect of the PNB. The scattering of the probe laser beam by the nanobubble reduces the axial intensity of the probe laser and results in a dip-shaped trace that showed the expansion and collapse of the nanobubble as a bubble-specific time course (Figure S1B). The duration of scattering trace is measured at the half level of its minimum with 0.4 ns resolution and is defined as a lifetime of the nanobubble. The level of laser pulse fluence that corresponds to the probability of PNB generation of 0.5 was determined as the threshold of the nanobubble generation.

Time-resolved scattering images (Figure S1C) were obtained with a short laser pulse (576 nm) delayed for 10 ns relative to the excitation pulse to allow formation and expansion of the nanobubble (Figure S1C). This probe laser side-illuminates the sample so that only light scattered by the nanobubble is collected by the microscope objective lens and projected onto an image detector (Luka model, Andor Technology, Northern Ireland). The image of the PNB is then used to determine the location of the nanobubble relative to the cell and the location of the

NP clusters. Cancer cells are identified with fluorescent microscopy imaging using a GFP-specific green fluorescence since the cancer cell line was transfected with green fluorescent protein (GFP). Optical scattering images of gold NP clusters were obtained using the same method as for the imaging of PNBs. NP cluster images were obtained in the absence of the excitation laser pulse. The above three imaging modes coupled with bright field microscopy allowed us to identify cancer cells, NP clusters, PNBs and to correlate the location of PNBs vs that of gold NP clusters and cancer cells in *in vitro* model.

Acoustic detection of the PNB (Figure S1D) employed XMS-310 ultrasound transducer (Olympus NDT Inc., Waltham, MA) coupled to pre-amplifier (Ultrasonic *Preamp 5676,* Olympus NDT Inc., Waltham, MA). The output of the amplifier was registered as the acoustic response of the nanobubble with the oscilloscope. To correlate acoustic and optical methods of the nanobubble detection we have measured the amplitude of the acoustic response as function of the nanobubble lifetime measured optically. The experiment was performed for individual cells and the acoustic and optical responses were simultaneously detected during exposure of each individual cell to a single laser pulse. We observed almost a liner correlation between these two parameters and this justified using acoustic amplitude instead of the nanobubble lifetimes in opaque tissues (these procedure and data are described in detail in ref. [S7]. In the animal experiment the ultrasound transducer was pressed to a tissue through an ultrasound gel (Aquasonic 100, Parker Laboratories, Inc., Fairfield, NJ) at the distance of 2-3 mm from the irradiated area.

4. Cell model. We used multi drug-resistant HN31 squamous carcinoma cells (associated with head and neck cancers) expressing EGFR and immortalized normal human oral kerotinocyte NOM9 cells. The NOM9 cells were cultured in KGM Complete Medium (Cat# CC-3001) from

Lonza in a 37°, 5% CO_2 incubator. The malignant cells were transfected with GFP to allow identification. The HN31 GFP stable cell line was built by transfecting the EGFP C1 plasmid into HN31 cells. The selecting marker was G418. The transfected cells were cultured in DMEM High Glucose medium (Cat# 10013 CV) from Mediatech supplemented with MEM Vitamin Solution (Cat# 11120) and MEM NEAA (Cat#11140) both from Gibco and penicillin-streptomycin (Cat# 30002 CT) from Mediatech in the same incubator. For co-culture, the cells were resuspended in KGM media and counted after trypsinization and neutralization. NOM 9 was mixed with HN31 GFP cell in 100:1 ratio and seeded at a density of 700,000 cells/ml in 15-well chambered slide (µ-Slide Angiogenesis, Ibidi LLC, Martinsried, Germany). Cell death was measured with Trypan Blue exclusion test in 72 hours after the treatment.

We used stock encapsulated anti-tumor drug, Doxil (Doxorubicin encapsulated into 85 nm liposomes). The Doxil liposomes (Ben Venue Laboratories, Inc, Bedford, OH) were also conjugated with the same antibody (C225) as described in [S8-S10] for their active targeting and endocytosis by cancer cells. Conjugated gold NPs ($2.4*10^{10}$ particles/ml) and Doxil liposomes (in variable concentration of doxorubicin from 1 to 100 µg/ml) were separately administered *in vitro* by incubating for 24 hour with a co-culture of HN31/NOM9 cells under physiological conditions (37ºC). After that uncoupled NPs and liposomes were washed off prior to the exposure to laser pulse. Small size of NPs (60 nm) and of liposomes (85 nm) provided efficient targeting through receptor-mediated endocytosis of both components. As a result of such targeting NPs and Doxil liposomes were selectively internalized by target cells and formed mixed intracellular clusters (as was also established previously [S7, S11-S14]), likely within endo-lysosomal system in cytoplasm (Figure 2A). Uptake of NPs and Doxil by living cells was assayed with a confocal microscopy (LSM-710, Carl Zeiss MicroImaging GmbH, Germany) in

the bright field, optical scattering (for imaging of gold NPs, shown in *blue* color in Figure 2A) and two fluorescent (for a separate imaging of GFP in cancer cells at 520 nm (Figure S2A) and Doxil at 605 nm (*red* color in Figure S2A)) modes. Cancer cells were identified among normal cells in a co-culture through their green GFP-specific fluorescence.

5. Animal model. Healthy, male athymic nude mice, age 8 to 12 weeks, were used in our experiments and they were purchased from the animal production area of the National Cancer Institute-Frederick Cancer Research and Development Center (Frederick, MD). A xenograft model, in which the tumor cells are implanted in the tumor site of origin, was used. The tumors were induced with the human head and neck squamous carcinoma HN31 cells on the mice flanks: the nude mice were anesthetized and $1x10^6$ HN31 cells were injected using a 1-ml tuberculin syringe with a 30-gauge hypodermic needle. 14 to 17 days after the injection of cells, when tumors are already established (5-6 mm in diameter), the C225-conjugated 60 nm gold spheres diluted by serum-free Dulbecco's modified Eagle's medium were slowly injected as:

- intravenous (systemic) delivery: the mice were kept under anesthesia and the gold NP-C225 conjugates in 200 μl (concentration was 0.8μg/g of body weight) were slowly injected into mice via the tail vein using an intravenous catheter and a 1-ml-insulin-syringe.
- Local (intra-tumor) delivery: the mice were kept under anesthesia and the gold NP-C225 conjugates in 1 μl (concentration was 0.8μg/g) were slowly injected in 1-2 points at the rate of 500 nl/min using a 5-μl syringe with a 26-gauge needle and a syringe pump (**NE-1000, New Era Pump Systems,** Wantagh, NY).
- Doxil was injected locally: the mice were kept under anesthesia and the Doxil in 1 μl (concentration was 1 mg/kg) was injected in the same 1-2 points of the tumor (injection rate was 500 nl/min).

24 h after injection of gold NP-C225 conjugated and drug, laser treatment of the animals were done. For this, the mice were anesthetized and a skin was removed in an area of laser treatment (tumor and adjacent tissue). Laser beam was scanned across the surface of the tumor and normal tissue at the speed 0.62 mm^2/s. Scan speed, beam diameter and pulse repetition rate (20 Hz) were synchronized in order to provide a single pulse exposure mode for each area of the tumor and tissue. To provide better optical and acoustic contact between optical fiber tip, acoustic detector and the tumor surface we applied transparent gel (Aquasonic 100, Parker Laboratories, Inc., Fairfield, NJ).

Five different treatment modes were studied: small PNBs (40 mJ/cm^2 @780 nm, single pulse, NP: gold 60 nm spheres w/C225) + Doxil (D:1 mg/kg); PNBs alone; Doxil+NP, Doxil alone and no treatment. Each treatment mode was repeated for 3-6 animals that received identical NP, drug and laser treatment. Half of the tumor was irradiated while the other half was used as un-irradiated control. This allowed us to reduce the number of animals employed. The duration of laser treatment of the whole animal (including several scans) did not exceed several minutes. Animal were transported to and from the laser set up by M. D. Anderson Cancer Center staff in accordance with the Animal Care and Use Guidelines of M. D. Anderson Cancer Center. The mice were housed and maintained in laminar flow cabinets under specific pathogen-free conditions in facilities of the M. D. Anderson Cancer Center. These facilities were approved by the American Association for Accreditation of Laboratory Animal Care in accordance with current regulations and standards of the U.S. Department of Agriculture, the U. S. Department of Health and Human Services, and the National Institutes of Health. All procedures causing discomfort were performed under anesthesia (an intraperitoneal injection of a 1.2% avertin solution, 0.2ml/10g body weight). Mice were observed daily for their level of activity and

normal eating, drinking and grooming behavior. If a mouse demonstrated marked weight loss, had ruffled fur and showed difficulty walking, it was removed from the study and euthanatized with carbon dioxide gas. This method of euthanasia is consistent with the guidelines set by the panel on Euthanasia of the American Veterinary Medical Association.

Tissue viability was analyzed in 72 h after laser irradiation. The irradiated and intact tumors were extracted, fixed with 10% formalin for 48 h, embedded in paraffin and prepared by standard technique for hematoxylin-eosin (H&E) staining. For analysis of tissue necrosis, the tumors were sliced in a direction of propagation of laser radiation. The necrosis level of tumor and normal tissue was measured in slices (Figure 5A-C) in the direction of laser beam propagation as a function of tissue depth in the range from 0 mm (surface) to 2 mm depth. The necrosis level was calculated as the ratio of the areas of necrotic tumor (tissue) to the whole area of the tumor (tissue) and multiplied by 100%.

6. Validation of the PNB signals and optimization of the excitation wavelength. The above PNB signals and metrics were validated for cells and *in vivo* models. Optical scattering imaging was obtained for cancer and normal cells. Scattering images of gold NPs in cells were correlated to the fluorescent images of cancer cells (Figure S2A) and to the images of PNBs in the same cells (Figure S2B). Thus we linked the origin of PNBs to the largest gold NP clusters that were found only in cancer cells. PNBs were observed mainly in cancer but not in normal cells under identical treatment with gold NPs and laser pulses. The selectivity of the PNB generation in cancer cells was further validated for PNB lifetime that was derived from optical scattering responses obtained for the same cancer and normal cells (Figure S2C). For the wide range of fluence of the excitation laser pulse we observed significant difference in lifetimes of PNBs in cancer and normal cells (Figure S2E). In many cases we did not detect any PNBs at all in normal

cells (Figure S2B). The linear dependence of the PNB lifetime in cancer cells upon laser fluence indicated that the PNB size (characterized through the lifetime) can be precisely controlled through the fluence of laser pulse (Figure S2E). Acoustic responses of PNBs were obtained simultaneously with the optical responses and the acoustic amplitudes were correlated to the lifetimes of the same PNBs (Figure S2D). Observed correlation of acoustic and optical signals allowed to employ acoustic amplitude as a metric of the maximal size of the PNB in opaque tissue (typical for animal model) where optical signals are significantly attenuated and distorted.

Next, in order to optimize the laser wavelength for the near-infrared excitation the acoustic amplitudes of PNBs were obtained as the spectra of the excitation laser wavelength in cancer cells *in vitro* and in tumor and normal tissue in animals that received intravenous gold NP-C225 conjugates and for a intact tumor in animals that did not receive any gold NPs (Figure S3 and Figure 4C). The follow up exposure of individual living cells to single laser pulses resulted in PNB-specific time-responses that also showed narrow NIR peaks at 780 nm (Figure S3). Spectra of amplitudes of acoustic responses were obtained for a tumor and normal tissue of the NP-treated animal in a single laser pulse excitation mode at 40 mJ/cm^2 (Figure 4C). The tumor in the NP-treated animal showed a 3 nm wide peak also at 780 nm with the acoustic signal amplitude at 780 nm being close to that at 532 nm. Other NIR wavelengths returned much lower signals comparable to the background level. The normal tissue of the NP-treated animal showed very small acoustic signals that were also comparable to the background level, while intact tumor returned zero signals under identical optical excitation (Figure 4C). We concluded that the detected acoustic signals of the NP-treated tumor were associated with gold NPs that were selectively accumulated in the tumor cells *in vivo*. We therefore employed the near-infrared wavelength of 780 nm for the experiments *in vitro* and *in vivo*.

REFERENCES

S1. Lukianova-Hleb EY, Lapotko DO. influence of transient environmental photothermal effects on optical scattering by gold nanoparticles. *Nano Lett.* 2009;**9**:2160-6.

S2. Hleb EY, Hu Y, Drezek RA, Hafner JH, Lapotko DO. Photothermal bubbles as optical scattering probes for imaging living cells. *Nanomedicine.* 2008;**3**:797-812.

S3. Lukianova-Hleb EY, Hu Y, Latterini L, Tarpani L, Lee S, Drezek RA, *et al.* Plasmonic nanobubbles as transient vapor nanobubbles generated around plasmonic nanoparticles. *ACS Nano.* 2010;**4**:2109-23.

S4. Neumann J, Brinkmann R. Nucleation dynamics around single microabsorbers in water heated by nanosecond laser irradiation. *J Appl Phys.* 2007;**101**:114701.

S5. Vanleeuwen TG, Jansen ED, Motamedi M, Welch AJ, Borst C. Excimer-laser ablation of soft-tissue - a study of the content of rapidly expanding and collapsing bubbles. *IEEE J Quantum Elect*. 1994;**30**:1339-47.

S6. Vogel A, Noack J, Huttman G, Paltauf G. Mechanisms of femtosecond laser nanosurgery of cells and tissues. *Appl Phys B-Lasers O.* 2005;**81**:1015-47.

S7. Lukianova-Hleb EY, Ren X, Zasadzinski JA, Wu X, Lapotko D. Plasmonic nanobubbles enhance efficacy and selectivity of chemotherapy against drug-resistant cancer cells. *Adv. Mater.* 2012;**24**:3831-7.

S8. Mamot C, Drummond DC, Greiser U, Hong K, Kirpotin DB, *et al.* Epidermal growth factor receptor (EGFR)-targeted immunoliposomes mediate specific and efficient drug delivery to EGFR- and EGFRvIII-overexpressing tumor cells. *Cancer Res.* 2003;**63**:3154-61.

S9. Lukyanov AN, Elbayoumi TA, Chakilam AR, Torchilin VP. Tumor-targeted liposomes:

doxorubicin-loaded long-circulating liposomes modified with anti-cancer antibody. *J Control Release.* 2004;**100**:135-44.

S10. Elbayoumi TA, Torchilin VP. Enhanced cytotoxicity of monoclonal anticancer antibody 2C5-modified Doxorubicin-loaded PEGylated liposomes against various tumor cell lines. *European Journal of Pharmaceutical Sciences*. 2007;**32**:159-68.

S11. Chithrani BD, Chan CW. Elucidating the mechanism of cellular uptake and removal of protein-coated gold nanoparticles of different sizes and shapes. *Nano Lett.* 2007;**7**:1542-50.

S12. Salmaso S, Caliceti P, Amendola V, Meneghetti M, Magnusson JP, Pasparakis G, *et al.* Cell up-take control of gold nanoparticles functionalized with a thermoresponsive polymer. *J Mater Chem* 2009;**19**:1608-15.

S13. Lukianova-Hleb EY, Hanna EY, Hafner JH, Lapotko DO. Tunable plasmonic nanobubbles for cell theranostics. *Nanotechnology.* 2010;**21**;82102.

S14. Lapotko DO, Lukianova-Hleb EY, Oraevsky AA. Clusterization of nanoparticles during their interaction with living cells. *Nanomedicine (Lond).* 2007;**2**:241-53.

Supplementary figures

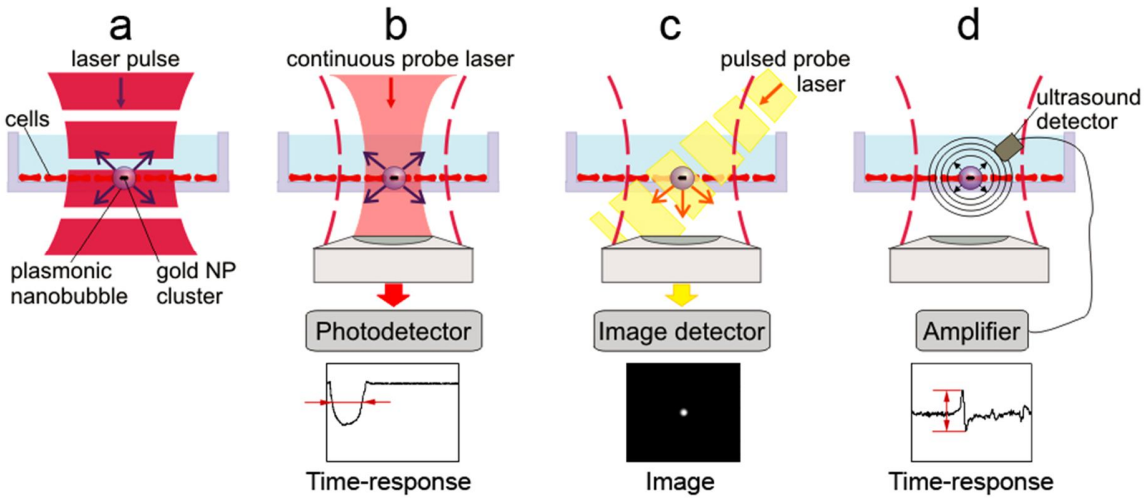

Figure S1. Experimental set up for generation and detection of plasmonic nanobubbles (PNBs). (**A**) Generation of a plasmonic nanobubble around gold NP cluster inside cancer cell due to absorption of a single short laser pulse (70 ps, 780 nm) by the gold NPs includes highly localized and rapid heating and vaporization of the liquid surrounding the NP cluster and the follow up explosive expansion and collapse of the PNB. (**B**) Optical scattering time-response of the PNB is obtained with a continuous probe laser (633 nm) that is focused into a sample collinearly with the excitation pulse. The scattering effect of the PNB reduces the axial intensity of the probe beam, which is measured by a fast photodetector and delivers the PNB lifetime (shown with red arrows). (**C**) Time-resolved optical scattering imaging employs side illumination with a probe laser pulse (70 ps, 580 nm, 2 nJ) that is delayed for 10 ns relative to the excitation pulse. The probe light is scattered by the PNB and forms a distinct image in the microscope that delivers the pixel image amplitude. (**D**) An acoustic time-response is obtained with an ultrasound transducer that remotely detects pressure transients emitted during PNB expansion and collapse and delivers acoustic amplitude of PNB (shown with red arrows).

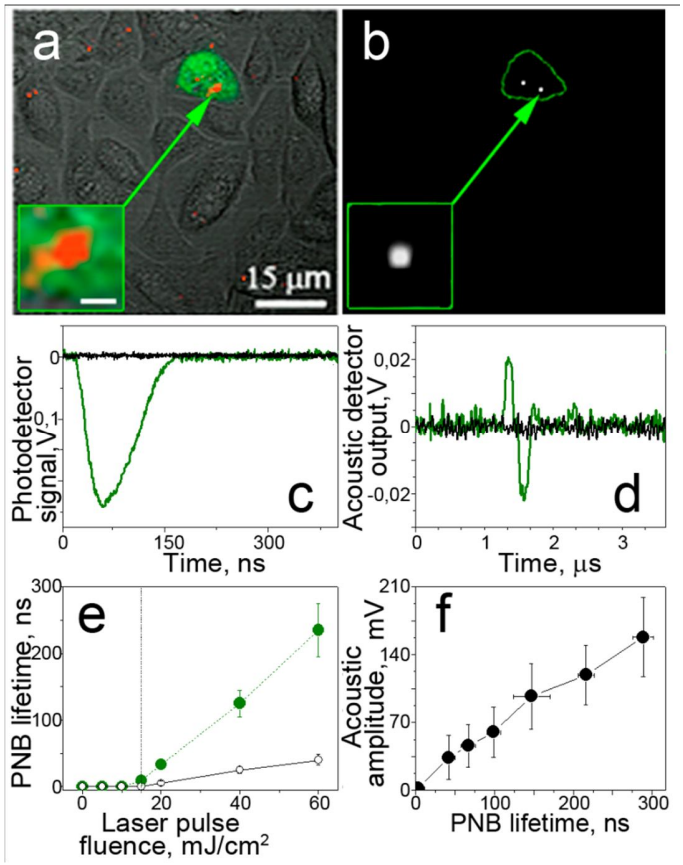

Figure S2. Generation of PNB in the mixed co-culture of HNSCC (*green*) and normal cells targeted with NP-C225. (**A**): Overlay of bright field, green fluorescent and scattering (*red*) images of the co-culture of NP-targeted HN31 and NOM9 cells; a large NP cluster in HN31 cell (inset) and non-specifically taken gold NPs can be seen. (**B**) Time-resolved optical scattering image of the same cells as in (**A**) show PNBs in HN31 cells during exposure to single laser pulse (70 ps, 780nm, 40 mJ/cm^2). (**C**) Quantified detection of PNB with optical scattering response. (**D**) Quantified detection of PNB with acoustic response that in HNSCC (*green*) and normal (*black*) cells. (**E**) Dependence of PNB lifetime upon laser pulse fluence (pulse energy/cm^2) for cancer (*solid green*) and normal (*hollow black*) cells. (**F**): Dependence of the acoustic response amplitude upon optically measured lifetime of PNBs.

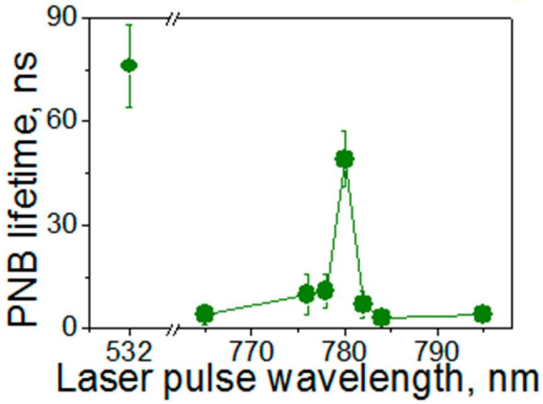

Figure S3. Spectrum of PNB lifetime obtained from individual squamous cell carcinoma cancer cells targeted with C225-conjugated 60 nm gold spheres (60 mJ/cm^2).